

# Diffusion Parameters of the Extracellular Space in Human Gliomas

LÝDIA VARGOVÁ,<sup>1,3</sup> ALEŠ HOMOLA,<sup>1,3</sup> JOSEF ZÁMEČNÍK,<sup>4</sup> MICHAL TICHÝ,<sup>5</sup>  
VLADIMÍR BENEŠ,<sup>6</sup> AND EVA SYKOVÁ<sup>1,2,3\*</sup>

<sup>1</sup>Department of Neuroscience, Charles University, Second Medical Faculty, Prague, Czech Republic

<sup>2</sup>Institute of Experimental Medicine, Academy of Sciences of the Czech Republic, Prague, Czech Republic

<sup>3</sup>Center for Cell Therapy and Tissue Repair, Charles University, Second Medical Faculty, Prague, Czech Republic

<sup>4</sup>Department of Pathology and Molecular Medicine, Charles University, Second Medical Faculty, Prague, Czech Republic

<sup>5</sup>Department of Neurosurgery, Charles University, Second Medical Faculty, Prague, Czech Republic

<sup>6</sup>Department of Neurosurgery, Charles University, First Medical Faculty, Prague, Czech Republic

**KEY WORDS**    apparent diffusion coefficient; brain tumors; extracellular space volume; malignancy

**ABSTRACT**    Tumor cell migration through the extracellular space (ECS) might be affected by its pore size and extracellular matrix molecule content. ECS volume fraction  $\alpha$  ( $\alpha$  = ECS volume/total tissue volume), tortuosity  $\lambda$  ( $\lambda^2$  = free/apparent diffusion coefficient) and nonspecific uptake  $k'$  were studied by the real-time tetramethylammonium method in acute slices of human tissue. The diffusion parameters in temporal cortical tissue resected during surgical treatment of temporal lobe epilepsy (control) were compared with those in brain tumors. Subsequently, tumor slices were histopathologically classified according to the grading system of the World Health Organization (WHO), and proliferative activity was assessed. The average values of  $\alpha$ ,  $\lambda$ , and  $k'$  in control cortex were 0.24, 1.55, and  $3.66 \times 10^{-3} \text{s}^{-1}$ , respectively. Values of  $\alpha$ ,  $\lambda$ , and  $k'$  in oligodendrogliomas did not significantly differ from controls. In pilocytic astroglomas (WHO grade I) as well as in ependymomas (WHO grade II),  $\alpha$  was significantly higher, while  $\lambda$  and  $k'$  were unchanged. Higher values of  $\alpha$  as well as  $\lambda$  were found in low-grade diffuse astrocytomas (WHO grade II). In cellular regions of high-grade astrocytomas (WHO grade III and IV),  $\alpha$  and  $\lambda$  were further increased, and  $k'$  was significantly larger than in controls. Classic medulloblastomas (WHO grade IV) had an increased  $\alpha$ , but not  $\lambda$  or  $k'$ , while in the desmoplastic type  $\alpha$  and  $k'$  remained unchanged, but  $\lambda$  was greatly increased. Tumor malignancy grade strongly corresponds to an increase in ECS volume, which is accompanied by a change in ECS structure manifested by an increase in diffusion barriers for small molecules. *GLIA* 42:77–88, 2003.

© 2003 Wiley-Liss, Inc.

## INTRODUCTION

Primary brain tumors (PBT) represent up to 2% of all malignant tumors in humans (Rubin and Farber, 1999). As the second most frequent pediatric tumor, and one of the common causes of cancer-related death in young adults, PBTs are of major clinical significance. Despite intensive study, many aspects of their biological behavior remain poorly understood.

It has been suggested that the biological behavior of PBT depends not only on the migratory properties of the tumor cells themselves, but also on the composition of the extracellular matrix (ECM) and the ability of

tumor cells to attach to the ECM, degrade it, and remodel the tissue structure (Chintala and Rao, 1996;

Grant sponsor: Grant Agency of the Czech Republic; Grant number: GACR 309/00/1430; Grant sponsor: Ministry of Education of the Czech Republic; Grant numbers: VZJ13/98; 1113000004; Grant sponsor: Academy of Sciences of the Czech Republic; Grant number: VZ AVOZ5039906; Ministry of Health of the Czech Republic; Grant numbers: VZ FNM 00000064203.

\*Correspondence to: Eva Syková, Institute of Experimental Medicine AS CR, Vídeňská 1083, 142 20 Prague 4, Czech Republic. E-mail: sykova@biomed.cas.cz

Received 1 October 2002; Accepted 27 November 2002

DOI 10.1002/glia.10204

Goldbrunner et al., 1999). Enlargement of the extracellular space (ECS) volume in human gliomas and meningiomas was suggested in earlier studies using electron microscopy (Bakay, 1970a) or the extracellular marker sucrose (Bakay, 1970b). Nicholson and Syková (1998) showed that the structure of nervous tissue may be fairly accurately revealed by the diffusion of substances in the ECS. Diffusion in the ECS of the nervous system is constrained by three factors (Nicholson and Phillips, 1981): the restricted volume of the selected tissue available for diffusing particles, i.e., the extracellular volume fraction  $\alpha$  ( $\alpha = \text{ECS volume/total tissue volume}$ ); tortuosity  $\lambda$  ( $\lambda^2 = \text{free/apparent diffusion coefficient}$ ), a factor describing hindrances to diffusion caused by cell processes; and finally, nonspecific uptake  $k'$ , a factor describing the loss of a substance across cell membranes.

In the present study, we examined all three ECS diffusion parameters in healthy human cortical tissue and in the most frequently appearing PBTs, namely, pilocytic astrocytomas, ependymomas, and medulloblastomas in children and diffuse astrocytomas of various grades and oligodendrogliomas in adults (Russell and Rubinstein, 1977). To investigate the relationship between the diffusion properties of tumor tissue and its proliferative activity, the ECS diffusion parameter values obtained by the real-time tetramethylammonium (TMA) iontophoretic method (Nicholson and Phillips, 1981) were subsequently correlated with proliferation markers such as the mitotic index and MIB-1 and phosphotopoisomerase II- $\alpha$  labeling indices.

## MATERIALS AND METHODS

### Slice Preparation

The measurements were performed on freshly resected brain tissue samples obtained from neurosurgery departments during surgical resection of brain tumors in 25 previously untreated male and female patients, aged 19 months to 68 years. As a control, we used cortical tissue that did not exhibit pathological changes, e.g., cell loss or astrogliosis, resected during surgical treatment of temporal lobe epilepsy from four patients aged 10–27 years. Informed consent was obtained from all patients, or from their guardians, in the case of children.

Immediately after tissue removal, samples were placed into ice-cold, bicarbonate-buffered transport solution bubbled with 95% O<sub>2</sub> and 5% CO<sub>2</sub> of the following composition (in mM): 134 mM NaCl, 1.25 mM K<sub>2</sub>HPO<sub>4</sub>, 26 mM NaHCO<sub>3</sub>, 3.3 mM MgCl<sub>2</sub>, and 20 mM glucose. Within 30 min after surgery, the tissue was mounted on a Vibratome stage, and 400- $\mu\text{m}$ -thick slices were cut in ice-cold solution. A slice was then placed into the experimental chamber and perfused with a continuously bubbled (95% O<sub>2</sub> and 5% CO<sub>2</sub>) calcium-containing solution (134 mM NaCl, 1.25 mM K<sub>2</sub>HPO<sub>4</sub>, 26 mM NaHCO<sub>3</sub>, 1.3 mM MgCl<sub>2</sub>, 2 mM CaCl<sub>2</sub>, 20 mM glucose) at a flow rate of 10 ml/min. In

the experimental chamber, the slice was slowly warmed up, and measurements were carried out at room temperature (22–24°C) at various locations in the slice at a depth of 200  $\mu\text{m}$ .

## Diffusion Measurements

The ECS diffusion parameters were studied by the real-time iontophoretic method described in detail previously (Nicholson and Phillips, 1981; Lehmenkühler et al., 1993; Syková et al., 1994). In brief, an extracellular marker that is restricted to the extracellular compartment is used, such as tetramethylammonium ions (TMA<sup>+</sup>, MW = 74.1), to which cell membranes are relatively impermeable. TMA<sup>+</sup> is administered into the tissue by iontophoresis and mimics the extracellular diffusion of small ions and molecules. The concentration of TMA<sup>+</sup> measured in the ECS by a TMA<sup>+</sup>-ion-selective microelectrode (ISM) is inversely proportional to the ECS volume. Double-barreled TMA<sup>+</sup>-ISMs were prepared by a procedure described in detail previously (Syková, 1992). In brief, the tip of the ion-sensitive barrel was filled with an ion exchanger (Corning 477317); the rest of the barrel was backfilled with 100 mM TMA<sup>+</sup>chloride. The reference barrel contained 150 mM NaCl. The TMA<sup>+</sup>-ISMs were calibrated in 0.01, 0.03, 0.1, 0.3, 1.0, 3.0, and 10.0 mM TMA<sup>+</sup> in a background of 3 mM KCl and 150 mM NaCl. Calibration data were fitted to the Nikolsky equation, to determine electrode slope and interference. The shank of the iontophoretic pipette was bent so that it could be aligned parallel to that of the ion-selective microelectrode and was backfilled with 100 mM TMA<sup>+</sup>chloride. An electrode array was made by gluing together a TMA<sup>+</sup>-ISM and an iontophoretic micropipette with a tip separation of 100–200  $\mu\text{m}$  (Fig. 1). The iontophoresis parameters were +20-nA bias current (continuously applied to maintain a constant electrode transport number), with an +180-nA current step of 60-s duration to generate the diffusion curve. The three parameters were extracted by a nonlinear curve-fitting simplex algorithm operating on the diffusion curve described in eq. (1), which represents the behavior of TMA<sup>+</sup>. It is assumed that it spreads out with spherical symmetry, when the iontophoresis current is applied for duration  $S$ . In this expression,  $C$  is the concentration of the ion at time  $t$  and distance  $r$  (distance from the source electrode). The equation governing diffusion in nervous tissue is:

$$C = G(t) \quad t < S, \quad \text{for the rising phase of the curve}$$

$$C = G(t) - G(t - S)$$

$$t > S, \quad \text{for the falling phase of the curve}$$

The function  $G(u)$  is evaluated by substituting  $t$  or  $t - S$  for  $u$  in the following equation:

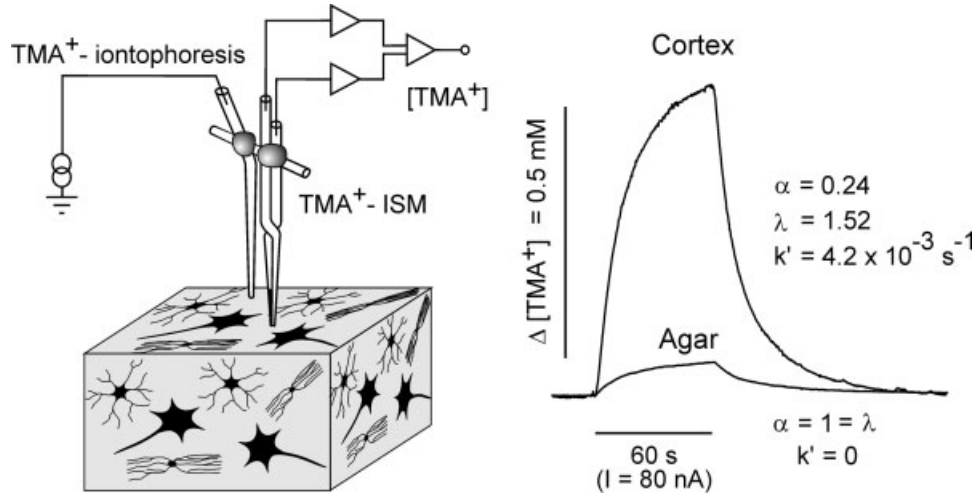


Fig. 1. Scheme of the experimental setup for diffusion measurements (left) and representative tetramethylammonium (TMA)<sup>+</sup>-diffusion curves obtained in agar gel and in healthy neocortical tissue (right). To stabilize the intertip distance of the electrode array, an iontophoretic micropipette and TMA<sup>+</sup>-selective microelectrode were

glued together with dental cement. In the brain, where diffusion is constrained by various barriers and is restricted to the extracellular space, the amplitude of the diffusion curve is much higher, and its shape differs from the diffusion curve measured in agar gel, where, by definition,  $\alpha = \lambda = 1$ , and  $k' = 0$ .

$$G(u) = (Q\lambda^2/8\pi D\alpha r) \{ \exp[r\lambda(k'/D)^{1/2}] \times \operatorname{erfc}[r\lambda/2(Du)^{1/2} + (k'u)^{1/2}] + \exp[-r\lambda(k'/D)^{1/2}] \times \operatorname{erfc}[r\lambda/2(Du)^{1/2} - (k'u)^{1/2}] \} \quad (1)$$

The quantity of TMA<sup>+</sup> delivered to the tissue per second is  $Q = In/zF$ , where  $I$  is the step increase in current applied to the iontophoresis electrode,  $n$  is the transport number,  $z$  is the number of charges associated with the substance iontophoresed (+1 here), and  $F$  is Faraday's electrochemical equivalent. The function  $\operatorname{erfc}$  is the complementary error function. Knowing  $n$  and  $D$ , the parameters  $\alpha$ ,  $\lambda$ , and  $k'$  can be obtained when the experiment is repeated in a tissue sample.

Before tissue measurements, diffusion curves were recorded in 0.3% agar gel (Difco, Detroit, MI) dissolved in a solution of 150 mM NaCl, 3 mM KCl, and 1 mM TMA chloride. In dilute agar,  $\alpha$  and  $\lambda$  are by definition set to 1, and  $k'$  is set to 0; the electrode transport number ( $n$ ) and the free TMA<sup>+</sup> diffusion coefficient ( $D$ ) are extracted by curve fitting.

### Morphology and Immunohistochemistry

The slices used for diffusion measurements and the remaining resected tissue were fixed in 10% buffered formalin and were then embedded in paraffin. To determine the morphological features of the tissue, routine hematoxylin and eosin (H&E) staining was carried out. Astrogliosis or the astrocytic nature of a neoplasm was demonstrated by positive immunostaining with antibodies directed against glial fibrillar acidic protein (GFAP).

Tissue sections were deparaffinized in xylene and rehydrated through decreasing concentrations of etha-

nol to water. After blocking of endogenous peroxidase activity, sections used for immunohistochemical staining were incubated overnight at 4°C with monoclonal anti-GFAP (Sigma-Aldrich; clone G-A-5, dilution 1:80). The antigen-antibody complexes were visualized using a Vectastain Elite Kit (Vector Laboratories).

As proliferation markers, we used Ki-67, an antigen that corresponds to a nuclear nonhistone protein expressed in all mitotic cell cycles except G0 (Brown and Gatter, 1990; Gerdes et al., 1991; Cattoretti et al., 1992), and phosphotopoisomerase II- $\alpha$  (topo II- $\alpha$ ), an enzyme that functions in chromosome segregation and condensation (Holm et al., 1989), and that has also been recently demonstrated to identify cells in the S, G2, and M phases of the cell cycle in human malignancies (Lynch et al., 1997). The immunostaining procedure for both topo II- $\alpha$  and Ki-67 has been described previously (Brown and Gatter, 1990; Lynch et al., 1997). Briefly, heat-induced epitope retrieval was done in a sodium citrate buffer solution (pH 9.0) warmed up to 97°C in a water bath for 40 min for topo II- $\alpha$  or heated for 30 min at high power in a microwave oven for Ki-67 (Gown et al., 1993). After subsequent cooling for 20 min and blocking of endogenous peroxidase, sections were incubated overnight at 4°C with either anti-topo II- $\alpha$  (Immunotech; mouse monoclonal antibody, clone 3D4, dilution 1:100) or anti-Ki-67 (Immunotech; mouse monoclonal antibody, clone MIB-1, dilution 1:50). A streptavidin-biotin kit (UltraTech HRP Detection System, Immunotech), followed by chromogenic visualization using diaminobenzidine, was used for immunolocalization of the antigens. All sections were lightly counterstained with Harris's hematoxylin, dehydrated, cleared, and mounted.

Only nuclear staining was regarded as positive in reactions with both the anti-topo II- $\alpha$  and the anti-

TABLE 1. Mean Values of the ECS Diffusion Parameters (Extracellular Volume Fraction,  $\alpha$ , Tortuosity  $\lambda$ , and Nonspecific Uptake  $k'$ ), Mitotic Index, and MIB-1 and Anti-topo-II- $\alpha$  Labeling Indices in Healthy Human Neocortical Tissue and Primary Brain Tumors of Different WHO Grades

No.	Age (yr)	Sex	Dx	$\alpha$	$\lambda$	$k'$ ( $\times 10^3 \text{s}^{-1}$ )	MI	MIB-1	Anti-topo II- $\alpha$	Tumor morphology	Tumor localization	Clinical notes (time of follow-up/clinical state)
1	10	F	c	0.24 $\pm$ 0.01	1.61 $\pm$ 0.01 n = 2, N = 7	2.57 $\pm$ 0.47	0	0.6	32.0	Temporal lobe neocortex		
2	10	F	c	0.23 $\pm$ 0.01	1.65 $\pm$ 0.01 n = 2, N = 6	1.41 $\pm$ 0.05	0	0.4	35.4	Temporal lobe neocortex		
3	17	F	c	0.24 $\pm$ 0.01	1.50 $\pm$ 0.02 n = 3, N = 8	1.87 $\pm$ 0.16	0	0.6	35.4	Temporal lobe neocortex		
4	26	M	c	0.24 $\pm$ 0.01	1.48 $\pm$ 0.02 n = 2, N = 6	8.57 $\pm$ 0.32	0	0.6	35.4	Temporal lobe neocortex		
5	2.5	F	a1	0.35 $\pm$ 0.01*	1.61 $\pm$ 0.01 n = 2, N = 5	3.31 $\pm$ 0.23	0	0.6	35.4	Alternating biphasic pattern (compact/microcystic)	Left optic nerve, before chiasm	3 years/alive, without recurrences
6	4	F	a1	0.37 $\pm$ 0.02*	1.52 $\pm$ 0.03 n = 3, N = 9	2.59 $\pm$ 0.78	0	0.4	35.4	Mostly microcystic structure	Suprasellar	3 years/alive, without recurrences
7	7	M	a1	0.38 $\pm$ 0.02*	1.52 $\pm$ 0.05 n = 3, N = 8	6.90 $\pm$ 0.82*	1	1.2	0.4	Mostly microcystic	Fourth ventricle	2 years/alive, without recurrences
8	17	M	a1	0.38 $\pm$ 0.01*	1.37 $\pm$ 0.01 n = 2, N = 6	7.80 $\pm$ 0.75*	0	1.6	2.2	Alternating biphasic pattern	Fourth ventricle	1.5 years/alive, without recurrences
9	10	M	a1	0.41 $\pm$ 0.02*	1.49 $\pm$ 0.01 n = 2, N = 6	4.96 $\pm$ 0.26	1	2.6	3.2	Mostly microcystic, mild perivascular edema	Fourth ventricle	2.5 years/alive, without recurrences
10	12	M	a2	0.27 $\pm$ 0.01	2.12 $\pm$ 0.07*	7.13 $\pm$ 1.03	0	3.8	4.4	High cellularity, dense fibrillary background	Right thalamus	2.5 years/alive, without recurrences
11	9	M	a2	0.31 $\pm$ 0.02*	1.69 $\pm$ 0.02* n = 5, N = 15	3.70 $\pm$ 0.50	1	6.6	7.2	High cellularity, fine fibrillary background	Left temporo-parietal	2.5 years/alive, without recurrences
12	26	M	a2	0.29 $\pm$ 0.01*	1.57 $\pm$ 0.02 n = 4, N = 12	3.13 $\pm$ 0.62	3	7.2	7.6	Low cellularity, few gemistocytes	Left frontal lobe	1.5 years/alive, without recurrences
13	47	F	a3	0.41 $\pm$ 0.01*	1.67 $\pm$ 0.03* n = 4, N = 11	5.12 $\pm$ 0.43	11	19.4	16.2	Low cellularity, mostly gemistocytes, mild perivascular edema, elongated cells with marked atypia	Left fronto-temporal	2 years/recurrence in 1.5 years, alive
14	8	F	a3	0.52 $\pm$ 0.02*	1.67 $\pm$ 0.03* n = 3, N = 9	5.49 $\pm$ 0.78	24	31.2	32.0	Moderate cellularity, elongated cells with marked atypia	Left temporal	1 year/unknown fate
15	24	F	a3	0.53 $\pm$ 0.01*	1.87 $\pm$ 0.03* n = 2, N = 6	9.93 $\pm$ 1.13*	26	33.4	35.4	Hypercellularity, elongated cells	Left temporo-parietal	1.5 years/recurrence in 14 months, alive
16	68	F	a4	0.40 $\pm$ 0.01*	1.72 $\pm$ 0.03* n = 2, N = 6	9.93 $\pm$ 0.76*	15	22.8	22.8	Hypercellularity with pleomorphic cells	Right temporo-parietal	0.5 year/dead of tumor
17	54	M	a4	0.40 $\pm$ 0.01*	1.85 $\pm$ 0.03* n = 5, N = 14	4.40 $\pm$ 0.52	14	24.4	21.4	Crowded small cells, vascular proliferations, necrosis	Left temporal	1.5 years/recurrence in 10 months, dead of tumor

18	43	M	a4	0.42 ± 0.01*	1.86 ± 0.03* n = 5, N = 13	7.87 ± 0.98*	21	23.0	19.4	Crowded pleomorphic cells, vascular proliferations, necrosis	Right temporal	1 year/alive, without recurrences
19	62	M	a4	0.56 ± 0.01*	1.35 ± 0.04 n = 2, N = 6	2.64 ± 0.05	23	29.6	30.4	Pleomorph vascular regions, numerous necrotic regions	Right temporal	1.5 years/recurrence in 1 year, alive
20	62	F	a4	0.58 ± 0.02*	1.69 ± 0.03* n = 3, N = 7	5.19 ± 0.32	32	52.2	45.4	Pleomorph elongated cells, vascular proliferations, large necrotic regions	Right parietal	1.5 years dead of tumor
21	50	M	o	0.22 ± 0.01	1.47 ± 0.01 n = 4, N = 13	3.69 ± 0.26	0	2.0		Closely packed polygonal cells, fine capillary network	Left temporo-parietal	2 years/alive, without recurrences
22	46	F	o	0.24 ± 0.01	1.49 ± 0.04 n = 3, N = 8	9.16 ± 0.42*	0	2.2	3.2	Polygonal cells, fine capillary network, calcifications	Left frontal	1 year/alive, without recurrences
23	2.5	M	e	0.38 ± 0.01*	1.55 ± 0.03 n = 6, N = 16	5.61 ± 0.87	2	5.8	7.8	Cellular subtype, numerous perivascular pseudorosettes	Third ventricle	2 years/alive, without recurrences
24	39	F	e	0.42 ± 0.05*	1.58 ± 0.02 n = 2, N = 6	7.66 ± 0.54*	4	14.8	13.6	Cellular subtype, numerous perivascular pseudorosettes	Right lateral ventricle	1 year/alive, without recurrences
25	12	M	m	0.32 ± 0.01*	1.57 ± 0.01 n = 4, N = 13	6.52 ± 0.57*	18	24.2	24.6	Crowded small oval cells, moderate perivascular edema	Fourth ventricle	2.5 years/alive, without recurrences
26	1.5	M	m	0.35 ± 0.01*	1.49 ± 0.03 n = 5, N = 18	4.60 ± 0.69	13	20.8	22.6	Crowded small oval cells	Fourth ventricle	2 years/recurrence in 6 months, alive
27	11	F	m	0.58 ± 0.03*	1.76 ± 0.08* n = 2, N = 6	6.84 ± 0.76*	19	33.2	41.2	Crowded small oval cells	Fourth ventricle	1 year/alive, without recurrences
28	17	M	m	0.22 ± 0.01	1.80 ± 0.02* n = 4, N = 12	3.89 ± 0.52	4	18.4	16.6	Desmoplastic subtype	Multifocal, infratentorial	4 months/dead of tumor
29	14	M	m	0.22 ± 0.01	1.90 ± 0.03* n = 3, N = 8	4.03 ± 0.26	7	18.2	17.0	Desmoplastic subtype	Fourth ventricle	2 years/dead of tumor

ECS, extracellular space; WHO, World Health Organization; No, individual patient number; Dx, diagnosis; c, control; a1, pilocytic astrocytoma (WHO I); a2, diffuse astrocytoma (WHO II); a3, anaplastic astrocytoma (WHO III); a4, glioblastoma (WHO IV); o, oligodendroglioma (WHO II); e, ependymoma (WHO II); m, medulloblastoma (WHO IV); M, male; F, female; MI, mitotic index; n, number of slices; N, number of measurements; \*Values significantly higher than the average of the control means,  $P < 0.05$ ; means ± SEM were calculated from all measurements (N).

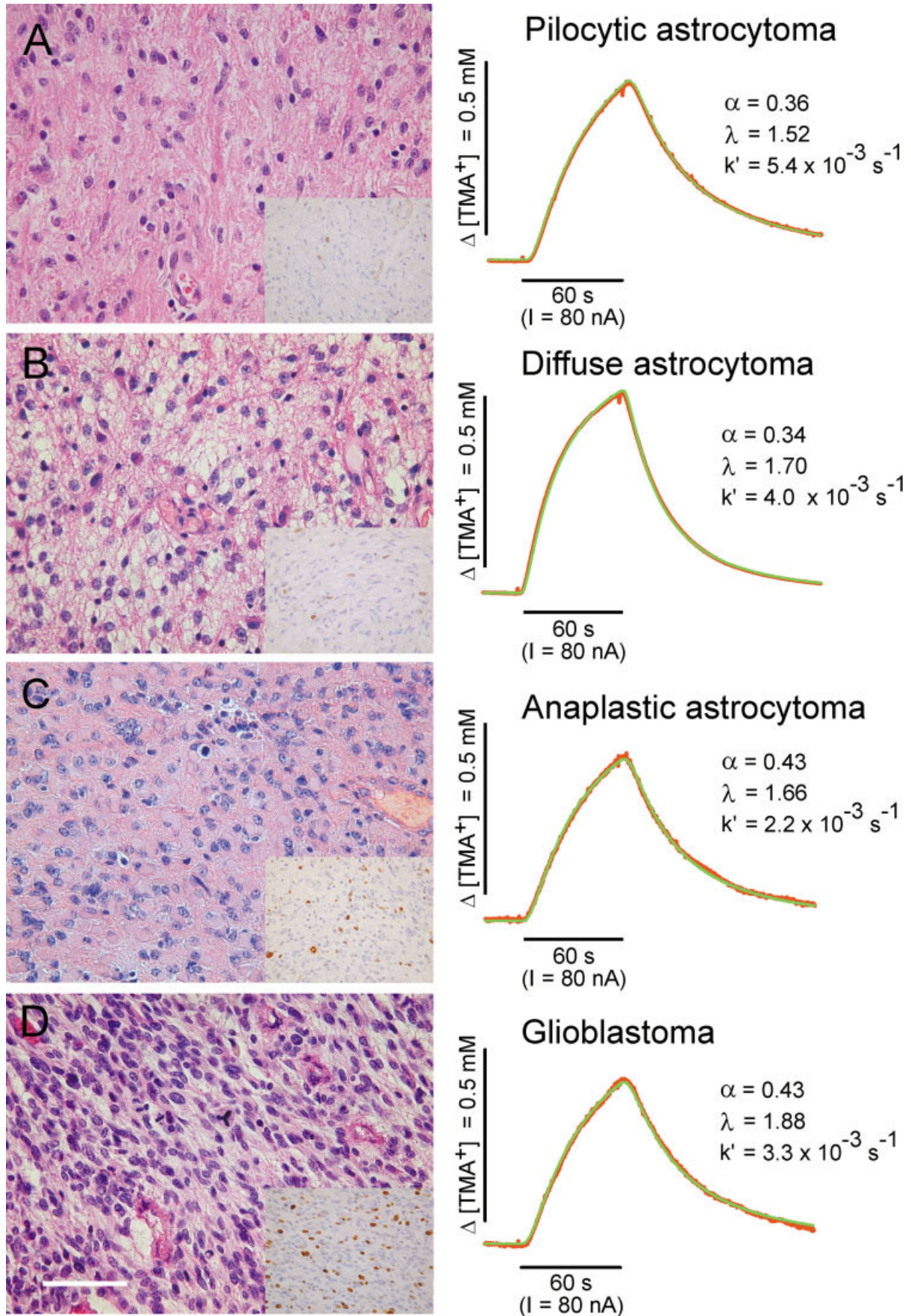


Figure 2.

Ki-67 antibodies. For the labeling indices (LI), positive nuclei were counted in 10 consecutive high-power fields (HPF)  $\times 400$  magnification in areas with the greatest staining; each count was divided by the number of tumor cells in the same HPFs (Kelleher et al., 1994). In the same 10 HPFs, all mitotic figures were counted, and their number was stated as the mitotic index (MI). Following conventional usage, the term MIB-1 labeling index is used in reference to the positive immunostaining for Ki-67 and the term anti-topo II- $\alpha$  labeling index is used in reference to the positive immunostaining for topo II- $\alpha$ .

### Statistical Analysis

The results of the experiments are expressed as mean  $\pm$  SEM. Statistical analysis of the differences between groups was performed using one-way analysis of variance (ANOVA). The correlation between the ECS diffusion parameter values and the MIB-1 labeling index was evaluated using the Pearson correlation coefficient  $r$ . Values of  $P < 0.05$  were considered significant.

## RESULTS

Tissue samples from 29 patients, 25 with diagnosed PBTs of various malignancy grades (20 gliomas and 5 medulloblastomas) and 4 surgically treated epileptic patients with mesiotemporal sclerosis were used. Measurements were performed in two to six slices from each tissue sample. In each slice, two to four diffusion measurements were done at different locations, and the obtained results were averaged (Table 1). The histological structure of the slices in the locations where the ECS diffusion parameters were measured was evaluated and correlated with the diffusion measurements. The results of diffusion measurements made in areas with hemorrhage, from near the edge of the tumor, from unaffected peritumorous tissue or from the vicinity of large vessels were excluded. The tumors were classified and graded according to the criteria outlined by the WHO (Kleihues and Cavenee, 2000) on the basis of an examination of the entire specimen. Cell proliferation was evaluated by the mitotic index (MI)

and the MIB-1 and anti-topo II- $\alpha$  labeling indices. A good correlation between the mitotic index, MIB-1 LI and anti-topo II- $\alpha$  LI was observed in all investigated cases (Table 1).

### Diffusion Parameters in Human Temporal Cortex

Measurements of the ECS diffusion parameters were performed in cortical layers III and IV of the temporal lobe neocortex. Only those values from samples with histologically verified normal tissue morphology, and without apparent astrogliosis, were used for statistical analysis (Fig. 1, Table 1, cases 1–4). The average values of  $\alpha$ ,  $\lambda$ , and  $k'$  in control tissue were  $0.24 \pm 0.01$ ,  $1.55 \pm 0.03$ , and  $3.66 \pm 0.98$  ( $\times 10^{-3} \text{s}^{-1}$ ), respectively (mean  $\pm$  SEM;  $n = 9$ ,  $n$  represents the number of slices).

### Pilocytic Astrocytomas

The prototypical pilocytic astrocytoma (WHO grade I, cases 5–9) was typically an architecturally and cytologically biphasic neoplasm with a varying proportion of compacted bipolar cells having Rosenthal fibers as well as loose-textured multipolar cells with microcysts and granular bodies (Fig. 2A). In pilocytic astrocytomas, the average values of  $\alpha$ ,  $\lambda$ , and  $k'$  were  $0.37 \pm 0.02$ ,  $1.50 \pm 0.03$ , and  $4.88 \pm 0.75 \times 10^{-3} \text{s}^{-1}$  ( $n = 12$ ), respectively. In comparison with control temporal cortex,  $\alpha$  in pilocytic astrocytomas was significantly higher, while  $\lambda$  and  $k'$  did not differ from control values (Table 1, asterisks). Mitotic activity as determined by mitoses counting and the MIB-1 and anti-topo II- $\alpha$  labeling indices (0–1, 0.4–2.6, and 0.4–3.2, respectively) was low (Table 1, Fig. 2A, inset).

### Diffuse Fibrillary Astrocytomas

WHO grade II diffuse astrocytomas exhibited a modest increase in cellularity and were characterized by the presence of an increased number of irregularly distributed astrocytes having discernible fibrillar processes. The tumor cells were only moderately atypical, and mitotic activity was either very low or absent (Fig. 2B). The ECS diffusion parameters were determined in three diffuse fibrillary astrocytomas (Table 1, cases 10–12). The average value of  $\alpha$  ( $0.29 \pm 0.01$ ;  $n = 14$ ) was significantly higher than that in control tissue but lower than that in pilocytic astrocytomas. Tortuosity was unusually high, with an average value of  $1.81 \pm 0.08$ . Extremely high tortuosity ( $>2.00$ ) was observed in case 10, in which a histological feature was a fascicularly arranged dense fibrillary background. In patients 11 and 12, such a dense fibrillary background was not found; indeed, the tortuosity values were not significantly different from those of controls. Nonspe-

Fig. 2. Left: Hematoxylin and eosin staining of the studied brain tumor tissues and the corresponding immunolabeling for Ki-67 to determine the MIB-1 labeling index (MIB-1 LI) shown in insets. Right: Representative tetramethylammonium (TMA)<sup>+</sup>-diffusion curves recorded in each distinct type of tumor with the corresponding values of the ECS diffusion parameters  $\alpha$ ,  $\lambda$ , and  $k'$ . Red curves, actual diffusion curves recorded in the tumor samples; green curves, theoretical diffusion curves generated by the nonlinear curve-fitting simplex algorithm (see Materials and Methods). **A:** Pilocytic astrocytoma (WHO grade I), MIB-1 LI 0.6 (case 9 in Table 1). **B:** Diffuse fibrillary astrocytoma (WHO grade II), MIB-1 LI 3.8 (case 11). **C:** Anaplastic astrocytoma (WHO grade III), MIB-1 LI 19.4 (case 13). **D:** Glioblastoma (WHO grade IV); cellular part, MIB-1 LI 23.0 (case 16). Scale bar = 50  $\mu\text{m}$ .

cific uptake  $k'$  in diffuse fibrillary astrocytomas did not differ from controls ( $4.77 \pm 0.89 \times 10^{-3}\text{s}^{-1}$ ). The mitotic index (0–3) and the MIB-1 (3.8–7.2) and anti-topo II- $\alpha$  (4.4–7.6) labeling indices showed slightly higher proliferative activity in diffuse fibrillary astrocytomas than in the pilocytic type, but the activity was still less than that seen in high-grade astrocytomas.

### Anaplastic Astrocytomas and Glioblastomas

The characteristic morphological features of anaplastic astrocytomas (WHO grade III) were increased cellularity, distinct nuclear and cellular pleomorphism, and marked mitotic activity (Fig. 2C). The histopathology of glioblastomas (WHO grade IV) was extremely variable (Fig. 2D). Glioblastomas were distinguished from anaplastic astrocytomas by the additional presence of extensive vascular proliferation and necrosis surrounded by dense palisading clusters of tumor cells (Fig. 3A). In glioblastomas, only values from the cellular parts of the tumors were used for statistical analysis; necrotic areas were evaluated separately.

In comparison with control and lower-grade astrocytomas,  $\alpha$  was substantially higher in high-grade astrocytomas (Table 1, cases 13–18), with an average value of  $0.44 \pm 0.01$  ( $n = 21$ ). The average values of  $\lambda$  and  $k'$  were significantly higher than those in controls ( $1.78 \pm 0.03$  and  $6.42 \pm 0.62 \times 10^{-3}\text{s}^{-1}$ , respectively). A marked increase in the number of mitoses (11–32) and the MIB-1 (19.4–52.2) and anti-topo II- $\alpha$  (16.2–45.4) labeling indices reflected the high proliferative activity and increased malignancy of the tumors (cases 13–20).

Measurements in the necrotic parts of two different glioblastomas (cases 19–20) demonstrated an enormously increased ECS volume ( $0.58 \pm 0.01$ ;  $n = 5$ ), while the tortuosity values varied widely (from 1.35 to 1.83). Nonspecific uptake  $k'$  in the necrotic parts of glioblastomas ( $4.15 \pm 0.62 \times 10^{-3}\text{s}^{-1}$ ) was lower than that in the cellular regions and did not differ significantly from average control values (Fig. 3A). In several necrotic regions, tortuosity did not decrease substantially as was expected, probably due to cell detritus, which prevents free diffusion.

To determine the relationship between the ECS diffusion parameters and the proliferative activity of the different diffuse astrocytomas (WHO II–IV), we plotted the  $\alpha$ ,  $\lambda$ , and  $k'$  values of the tested control and tumor tissue samples against the MIB-1 labeling index of the corresponding tumors (Fig. 4). Data from necrotic measurements (Table 1, cases 19 and 20) as well as data from patient 10 with a thalamic tumor were not incorporated into the plot. The histology of the tumor in case 10 was characterized by a fascicularly arranged dense fibrillary background, and therefore we assumed that diffusion in this sample was anisotropic; thus, the correct values of  $\alpha$  and  $\lambda$  could not be determined from measurements in one axis only (Rice et al., 1993; Mazel et al., 1998). Figure 4 shows a strong positive correlation of both increased ECS volume fraction  $\alpha$  and tor-

tuosity  $\lambda$  with increased proliferative activity (as expressed by the MIB-1 LI) in diffuse astrocytomas. The correlation coefficient ( $r$ ) of the regression curve for  $\alpha$  was  $r = 0.92$  ( $P < 0.0001$ ) and for  $\lambda$   $r = 0.68$  ( $P < 0.0001$ ). A similar correlation was also found between  $\alpha$ ,  $\lambda$ , and the mitotic and anti-topo II- $\alpha$  indices (not shown). Values of  $k'$  also correlated with increasing MIB-1 LI; the correlation coefficient of the regression curve for  $k'$  was  $r = 0.49$  ( $P < 0.002$ ).

### Oligodendrogliomas

Oligodendrogliomas were moderately cellular tumors with a dense capillary network composed of a sheet-like proliferation of uniform, round nuclei surrounded by optically clear halos (Fig. 3B). We tested two different oligodendrogliomas (WHO grade II) (Table 1, cases 20 and 21). The average values of  $\alpha$ ,  $\lambda$ , and  $k'$  ( $0.23 \pm 0.01$ ,  $1.50 \pm 0.032$ , and  $5.27 \pm 1.02 \times 10^{-3}\text{s}^{-1}$ , respectively;  $n = 7$ ) did not differ significantly from controls. The proliferative activity in the tested oligodendrogliomas was rather low and similar to that in low-grade astrocytomas (Table 1).

### Ependymomas

Ependymomas (WHO grade II) are moderately cellular gliomas. Their key histological feature was a collar-like condensing meshwork of fibrillary cytoplasmic processes about their stromal blood vessels in a formation known as perivascular pseudorosettes (Fig. 3C). In our study, we tested two ependymomas (Table 1, cases 22 and 23) and found a significantly increased  $\alpha$  ( $0.39 \pm 0.01$ ;  $n = 7$ ), but the values of  $\lambda$  ( $1.55 \pm 0.05$ ) and  $k'$  ( $5.3 \pm 1.06 \times 10^{-3}\text{s}^{-1}$ ) did not differ significantly from controls. The proliferative activity in the tested tumors was moderately increased (Table 1). The ependymoma with the higher proliferative activity (case 23) had a larger ECS volume than its counterpart (Table 1, Fig. 4).

### Medulloblastomas

Classic medulloblastomas were embryonal tumors forming densely packed masses composed of diminutive, undifferentiated-appearing cells with round-to-oval nuclei (Fig. 3D). In three tested classic medulloblastomas (Table 1, cases 24–26),  $\alpha$ ,  $\lambda$ , and  $k'$  varied substantially. In comparison with control tissue, we found a significant increase in the average  $\alpha$  value ( $0.38 \pm 0.03$ ;  $n = 11$ ), but not in the average  $\lambda$  or  $k'$  values:  $1.57 \pm 0.04$ ,  $5.82 \pm 0.62 \times 10^{-3}\text{s}^{-1}$ , respectively.

Tissue samples from patients 27 and 28 belonged to a rare desmoplastic subtype of medulloblastoma. These tumors displayed lower proliferative activity than was exhibited by the other medulloblastomas (Table 1), and their  $\alpha$  values ( $0.22 \pm 0.01$ ;  $n = 7$ ) were as low as those

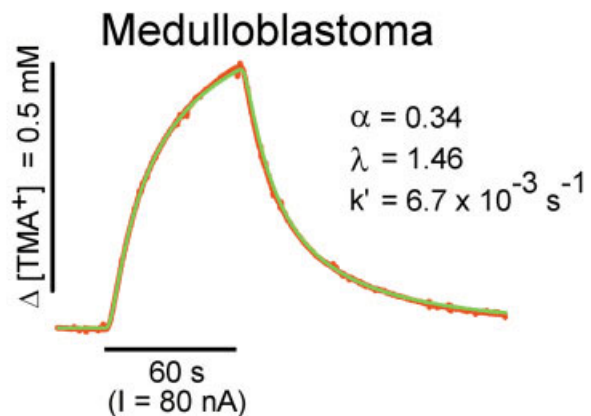
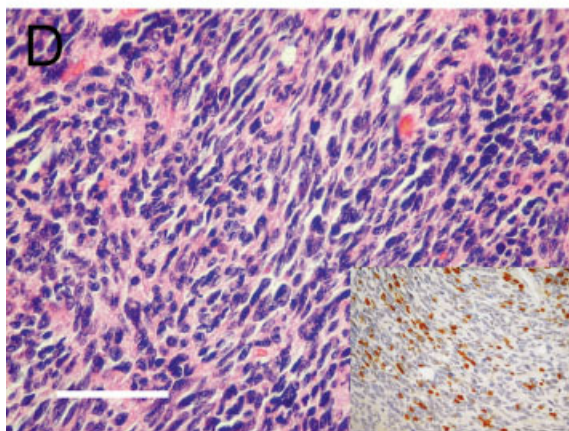
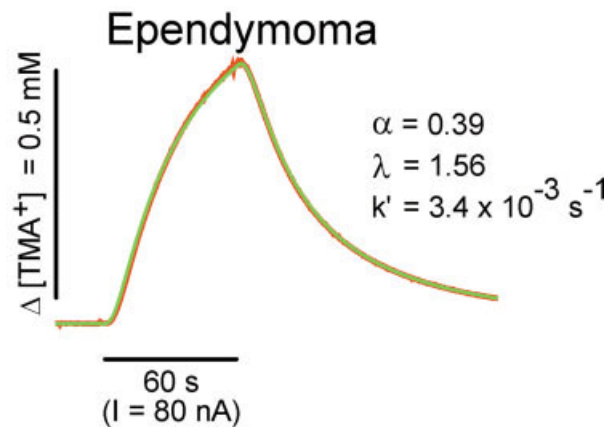
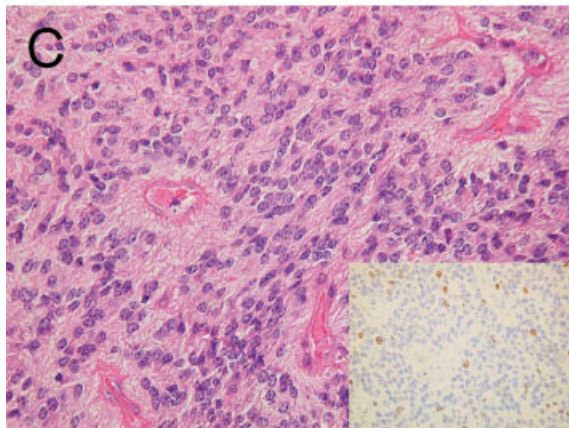
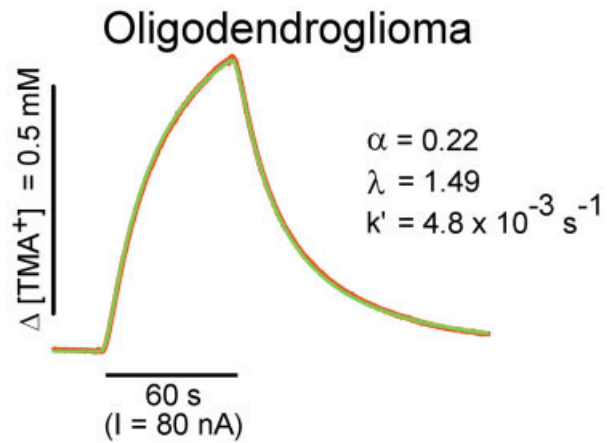
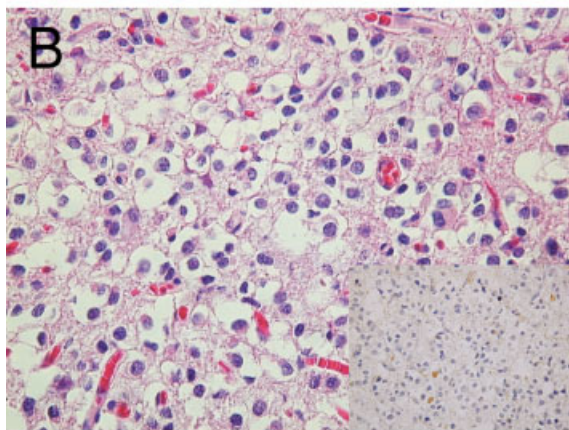
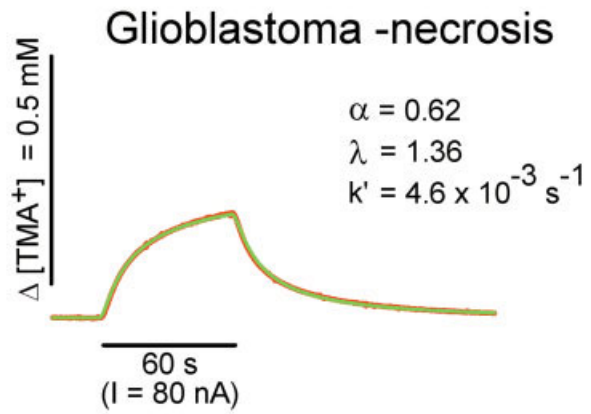
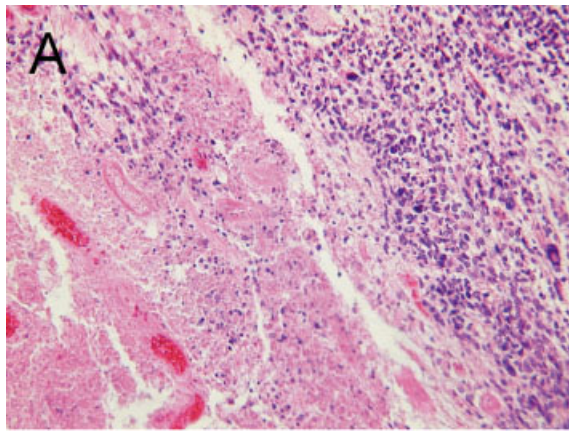


Fig. 3. Tumor tissue samples stained with hematoxylin and eosin with the corresponding MIB-1 immunostaining (insets) and representative tetramethylammonium (TMA)<sup>+</sup>-diffusion curves. Red curves, actual diffusion curves recorded in the tumor samples; green curves, theoretical diffusion curves generated by the nonlinear curve-fitting

simplex algorithm (see Materials and Methods). **A:** Glioblastoma (WHO grade IV); necrotic region (case19). **B:** Oligodendroglioma (WHO grade II), MIB-1 LI 2.2 (case 20). **C:** Ependymoma (WHO grade II), MIB-1 LI 7.8 (case 22). **D:** Medulloblastoma (WHO grade IV), MIB-1 LI 20.8 (case 26). Scale bar = 50  $\mu\text{m}$ .

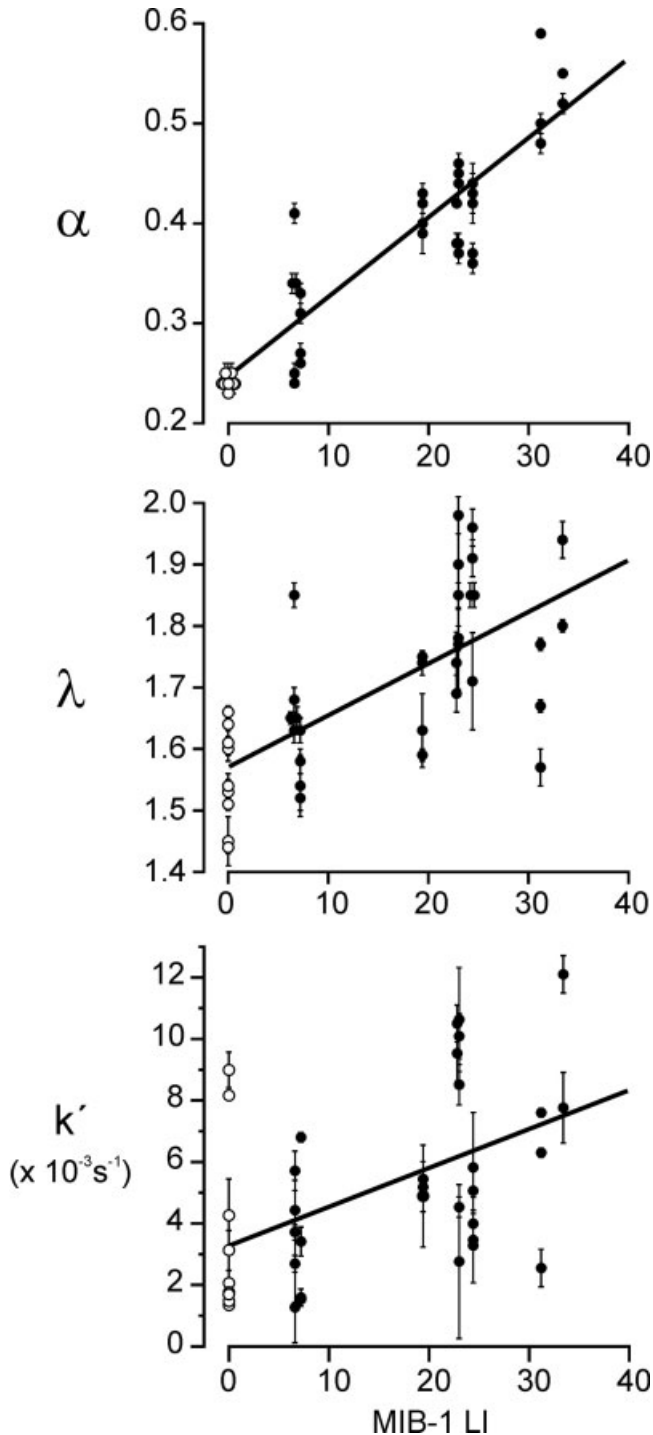


Fig. 4. Relationship between the extracellular space volume fraction  $\alpha$ , tortuosity  $\lambda$ , nonspecific cellular uptake  $k'$  and the MIB-1 labeling index in the studied diffuse astrocytomas (WHO II–IV; ●). Control data (○) are plotted against MIB-1 LI = 0. Each point represents an average value of  $\alpha$ ,  $\lambda$ , or  $k' \pm$ SEM calculated from 2–3 measurements in different slices. Slices from the same tumor have the same MIB-1 LI values. Regression curves for  $\alpha$ ,  $\lambda$ , and  $k'$  have correlation coefficients of 0.84, 0.46, and 0.24, respectively.

in healthy tissue. However, their tortuosity was enormously high ( $1.85 \pm 0.03$ ). Nonspecific uptake ( $4.00 \pm 0.41 \times 10^{-3} \text{ s}^{-1}$ ) did not differ from that of control tissue.

## DISCUSSION

The three ECS diffusion parameters,  $\alpha$ ,  $\lambda$ , and  $k'$ , govern the diffusion of substances in the ECS and affect synaptic as well as extrasynaptic transmission. They change during various physiological and pathological states (Syková et al., 2000; Syková, 2001). To the best of our knowledge, we have measured for the first time  $\alpha$ ,  $\lambda$ , and  $k'$  in human brain tissue and in primary brain tumors. The TMA<sup>+</sup> iontophoretic method is the only method that allows the absolute values of the three ECS diffusion parameters to be determined, since other methods provide information only about a single parameter or measure only their relative changes (for review, see Nicholson and Syková, 1998).

In control human temporal cortex from patients aged 10–27 years, we found a similar ECS volume fraction as has been observed in the central nervous system (CNS) of adult mice (Anděrová et al., 2001), rats (Lehmenkühler et al., 1993; Prokopová et al., 1997), or frogs (Prokopová-Kubinová and Syková, 2000). It has been shown repeatedly that the ECS diffusion parameters in CNS tissue slices obtained from experimental animals do not differ from those determined in animals in vivo (Lehmenkühler et al., 1993; Prokopová et al., 1997). We can assume that data from human tissue slices reflect the situation in human brain in vivo. From experiments on rodents, it is known that the ECS diffusion parameters vary dramatically during CNS development, due to tissue maturation during the first 3 postnatal weeks (Lehmenkühler et al., 1993; Prokopová et al., 1997), as well as during aging (Syková et al., 1998; Syková, 2001). Developmental magnetic resonance imaging (MRI) studies in humans showed a gradual change in T1- and T2-weighted images from an infantile to an adult-like pattern during the first 12 months of postnatal life, which is generally assumed to correspond with a decrease in water content in both gray and white matter and the period of myelination of the brain (for review, see Paus et al., 2001). One can therefore assume that the values of the ECS diffusion parameters in healthy tissue would also stabilize towards the end of the first year of life and that in children older than 1 year, they would not differ significantly from those in adults. Our youngest subjects were 1.5–4 years old (Table 1, cases 5, 6, 22, and 26), and the ECS diffusion parameter values in the cortical tissue of these children were not substantially different from those in adult patients.

Our measurements show that the ECS volume fraction  $\alpha$ , is increased in all the studied glial tumors and medulloblastomas except for oligodendrogliomas. We found a positive correlation between the size of the extracellular volume fraction and the malignancy grade of the tumors along with increasing cellularity and proliferative activity of the tumor as defined by the malignancy grading system (Kleihues and Cavenee, 2000). It is highly probable that structural changes in tumor tissue due to the degradation of the ECM by

metalloproteinases produced by tumor cells (Chintala et al., 1999) are responsible for the observed changes in this ECS diffusion parameter. All pilocytic astrocytomas, in spite of their low growth activity, had a large ECS volume fraction that might be due to the enlargement of the ECS by the numerous microcysts observed by microscopic examination. A loss of gap junctions, associated with a decrease in cell-cell communication (Trosko and Ruch, 1998; Soroceanu et al., 2001) and the ability of cells to regulate their volume (Quist et al., 2000), could also contribute to changes in ECS volume. An enlarged ECS volume, especially at the border between a tumor and the surrounding tissue, could result from neuronal death evoked by the excitotoxic effect of glutamate, which reaches unusually high concentrations in gliomas due to failed glutamate uptake (Ye et al., 1999; Ye and Sontheimer, 1999). The ECS volume fraction is not increased in oligodendrogliomas, tumors that do not actively kill peritumoral tissue. Indeed, glutamine synthetase, the enzyme that produces glutamate, is not expressed in oligodendrocytes; hence, these cells may be unable to release excitotoxic glutamate, as was shown in astrocytomas (Ye et al., 1999).

Surprisingly, the observed ECS volume increase was not associated with a decrease in tortuosity but, particularly in high-grade gliomas, with a significant tortuosity increase. It has been proposed that the migration of glioma cells may be facilitated by the molecules of the ECM (Harris, 1986). The production of certain ECM molecules, e.g., hyaluronic acid, chondroitin sulfate, or tenascin-C, by endothelial cells is increased and positively correlates with the migration of glioma cells and tumor invasiveness (Erickson and Bourdon, 1989; Knudson et al., 1989; Higuchi et al., 1993; Deryugina and Bourdon, 1996). Cell culture studies have shown that glioma cells are capable of producing their own ECM molecules, such as laminin, collagens, tenascin, vitronectin, and some glycosaminoglycans (Rutka et al., 1987, 1988; Delpech et al., 1993; Goldbrunner et al., 1999). The observed increase in tortuosity in our study may thus be the result of an increase in diffusion barriers formed by fine nets of overexpressed ECM molecules. TMA<sup>+</sup> diffusion parameters have been shown to be strongly dependent on the morphological structure of the tissue and the composition of the extracellular matrix (Syková et al., 1998, 1999; Roitbak and Syková, 1999; Voříšek et al., 2002). However, ion (TMA<sup>+</sup>) movement and cellular migration may have different requirements. While the movement of both is apparently enhanced by the increase in ECS volume, extracellular matrix molecules may specifically enhance cellular migration but hinder the diffusion of ions.

Unusually high values of tortuosity were observed in diffuse fibrillary astrocytomas (WHO grade II) with a dense fibrillary background (particularly case 10) and in desmoplastic medulloblastomas, which are characterized by distinctive reticulin-free islands of cells among reticulin-rich areas (cases 27 and 28). The high tortuosity values in these tumors may thus reflect the increased diffusion barriers formed by collagen or ret-

iculin fibers in the extracellular space. Moreover, fascicularly arranged fibers (case 10) may lead to uneven diffusion in different directions, i.e., to diffusion anisotropy (Rice et al., 1993; Mazel et al., 1998), with unusually high  $\lambda$  values in the direction in which the diffusion is limited.

MRI studies correlating the apparent diffusion coefficient of water ( $ADC_w$ ) with tumor grading and the degree of tumor cellularity showed that the value of  $ADC_w$  is inversely related to the malignancy of the tumor (Tien et al., 1994; Sugahara et al., 1999; Castillo et al., 2001; Kono et al., 2001). The authors assumed that a low  $ADC_w$  reflects a decreased ECS volume in hypercellular tumor tissue. In contrast, in early studies using extracellular markers such as sucrose, inulin, or radiotracers to determine ECS volume, investigators reported a larger ECS in animal or human brain tumors than in nonaffected tissue (Matthews and Molinaro, 1963; Bakay, 1970b; Ausman et al., 1977). In our study, together with an increase in ECS volume, we also observed an increase in tortuosity. In an animal model of nervous tissue injury, we have found that increased tortuosity due to an increased content of ECM molecules slows down  $ADC_w$  without any change in ECS volume (Voříšek et al., 2002). Tortuosity is, by definition, inversely related to ADC; thus, an increase in tortuosity reflects a lower ADC and the slower diffusion of ions and molecules due to diffusion barriers in the tumor environment. The relationship between  $ADC_w$  and tumor malignancy needs to be shown in MRI studies of patients with these tumors in order that MRI could prove a useful tool for diagnostic and therapeutic purposes.

The current study shows a positive correlation between increasing values of ECS volume fraction and proliferative activity in each distinct histological group of investigated tumors. We can therefore speculate that the malignancy of PBTs and their proliferative and migratory activity may also be dependent on the ability of the tumors to create space for migrating cells by the destruction of the surrounding tissue. Overexpression of certain ECM molecules has been shown to correlate with increased tumor malignancy and migratory activity (Zhang et al., 1998; Hayen et al., 1999; Camby et al., 2001), as these molecules may serve as "tracks" and thus facilitate tumor cell migration. However, they may form diffusion barriers for neuroactive molecules, including chemotherapeutics, which will constrain diffusion.

## REFERENCES

- Anděrová M, Kubinová S, Mazel T, Chvátal A, Eliasson C, Pekny M, Syková E. 2001. Effect of elevated K<sup>+</sup>, hypotonic stress, and cortical spreading depression on astrocyte swelling in GFAP-deficient mice. *Glia* 35:189–203.
- Ausman JI, Levin VA, Brown WE, Rall DP, Fenstermacher JD. 1977. Brain-tumor chemotherapy. Pharmacological principles derived from a monkey brain-tumor model. *J Neurosurg* 46:155–164.
- Bakay L. 1970a. The extracellular space in brain tumours. I. Morphological considerations. *Brain* 93:693–698.

- Bakay L. 1970b. The extracellular space in brain tumours. II. The sucrose space. *Brain* 93:699–708.
- Brown DC, Gatter KC. 1990. Monoclonal antibody Ki-67: its use in histopathology. *Histopathology* 17:489–503.
- Camby I, Belot N, Rorive S, Lefranc F, Maurage CA, Lahm H, Kaltner H, Hadari Y, Ruchoux MM, Brotchi J, Zick Y, Salmon I, Gabius HJ, Kiss R. 2001. Galectins are differentially expressed in supratentorial pilocytic astrocytomas, astrocytomas, anaplastic astrocytomas and glioblastomas, and significantly modulate tumor astrocyte migration. *Brain Pathol* 11:12–26.
- Castillo M, Smith JK, Kwok L, Wilber K. 2001. Apparent diffusion coefficients in the evaluation of high-grade cerebral gliomas. *AJNR Am J Neuroradiol* 22:60–64.
- Cattoretti G, Becker MH, Key G, Duchrow M, Schluter C, Galle J, Gerdes J. 1992. Monoclonal antibodies against recombinant parts of the Ki-67 antigen (MIB 1 and MIB 3) detect proliferating cells in microwave-processed formalin-fixed paraffin sections. *J Pathol* 168:357–363.
- Chintala SK, Rao JK. 1996. Invasion of human glioma: role of extracellular matrix proteins. *Front Biosci* 1:324–339.
- Chintala SK, Tonn JC, Rao JS. 1999. Matrix metalloproteinases and their biological function in human gliomas. *Int J Dev Neurosci* 17:495–502.
- Delpech B, Maingonnat C, Girard N, Chauzy C, Maunoury R, Olivier A, Tayot J, Creissard P. 1993. Hyaluronan and hyaluronectin in the extracellular matrix of human brain tumour stroma. *Eur J Cancer* 29A:1012–1017.
- Deryugina EI, Bourdon MA. 1996. Tenascin mediates human glioma cell migration and modulates cell migration on fibronectin. *J Cell Sci* 109:643–652.
- Erickson HP, Bourdon MA. 1989. Tenascin: an extracellular matrix protein prominent in specialized embryonic tissues and tumors. *Annu Rev Cell Biol* 5:71–92.
- Gerdes J, Li L, Schlueter C, Duchrow M, Wohlenberg C, Gerlach C, Stahmer I, Kloth S, Brandt E, Flad HD. 1991. Immunobiochemical and molecular biologic characterization of the cell proliferation-associated nuclear antigen that is defined by monoclonal antibody Ki-67. *Am J Pathol* 138:867–873.
- Goldbrunner RH, Bernstein JJ, Tonn JC. 1999. Cell-extracellular matrix interaction in glioma invasion. *Acta Neurochir (Wien)* 141:295–305; discussion 304–295.
- Gown AM, de Wever N, Battifora H. 1993. Microwave based antigenic unmasking: a revolutionary new technique for routine immunohistochemistry. *Appl Immunohistochem* 1:256–266.
- Harris AK. 1986. Cell traction in relationship to morphogenesis and malignancy. In: Steinberg MS, editor. *Developmental biology*. Vol 3. New York: Plenum. p 339–357.
- Hayen W, Goebeler M, Kumar S, Riessen R, Nehls V. 1999. Hyaluronan stimulates tumor cell migration by modulating the fibrin fiber architecture. *J Cell Sci* 112:2241–2251.
- Higuchi M, Ohnishi T, Arita N, Hiraga S, Hayakawa T. 1993. Expression of tenascin in human gliomas: its relation to histological malignancy, tumor dedifferentiation and angiogenesis. *Acta Neuro-pathol (Berl)* 85:481–487.
- Holden JA, Townsend JJ. 1999. DNA topoisomerase II-alpha as a proliferation marker in astrocytic neoplasms of the central nervous system: correlation with MIB1 expression and patient survival. *Mod Pathol* 12:1094–1100.
- Holm C, Stearns T, Botstein D. 1989. DNA topoisomerase II must act at mitosis to prevent nondisjunction and chromosome breakage. *Mol Cell Biol* 9:159–168.
- Kelleher L, Magee HM, Dervan PA. 1994. Evaluation of cell-proliferation antibodies reactive in paraffin sections. *Appl Immunohistochem* 2:164–170.
- Kleihues P, Cavenee WK. 2000. WHO classification of tumours. Pathology and genetics. Tumours of the nervous system. Lyon: IARC Press.
- Knudson W, Biswas C, Li XQ, Nemecek RE, Toole BP. 1989. The role and regulation of tumour-associated hyaluronan. *Ciba Found Symp* 143:150–159; discussion 159–169, 281–155.
- Kono K, Inoue Y, Nakayama K, Shakudo M, Morino M, Ohata K, Wakasa K, Yamada R. 2001. The role of diffusion-weighted imaging in patients with brain tumors. *AJNR Am J Neuroradiol* 22:1081–1088.
- Lehmenkühler A, Syková E, Svoboda J, Zilles K, Nicholson C. 1993. Extracellular space parameters in the rat neocortex and subcortical white matter during postnatal development determined by diffusion analysis. *Neuroscience* 55:339–351.
- Lynch BJ, Guinee DG Jr, Holden JA. 1997. Human DNA topoisomerase II-alpha: a new marker of cell proliferation in invasive breast cancer. *Hum Pathol* 28:1180–1188.
- Matthews CM, Molinaro G. 1963. A study of the relative value of radioactive substances used for brain tumor localization and of the mechanism of tumor: brain concentration. Uptake in transplantable fibrosarcoma, brain and other organs in the rat. *Br J Exp Pathol* 44:260–277.
- Mazel T, Šimonová Z, Syková E. 1998. Diffusion heterogeneity and anisotropy in rat hippocampus. *NeuroReport* 9:1299–1304.
- Nicholson C, Phillips JM. 1981. Ion diffusion modified by tortuosity and volume fraction in the extracellular microenvironment of the rat cerebellum. *J Physiol (Lond)* 321:225–257.
- Nicholson C, Syková E. 1998. Extracellular space structure revealed by diffusion analysis. *Trends Neurosci* 21:207–215.
- Paus T, Collins DL, Evans AC, Leonard G, Pike B, Zijdenbos A. 2001. Maturation of white matter in the human brain: a review of magnetic resonance studies. *Brain Res Bull* 54:255–266.
- Prokopová Š, Vargová L, Syková E. 1997. Heterogeneous and anisotropic diffusion in the developing rat spinal cord. *NeuroReport* 8:3527–3532.
- Prokopová-Kubinová Š, Syková E. 2000. Extracellular diffusion parameters in spinal cord and filum terminale of the frog. *J Neurosci Res* 62:530–538.
- Quist AP, Rhee SK, Lin H, Lal R. 2000. Physiological role of gap-junctional hemichannels. Extracellular calcium-dependent isosmotic volume regulation. *J Cell Biol* 148:1063–1074.
- Rice ME, Okada YC, Nicholson C. 1993. Anisotropic and heterogeneous diffusion in the turtle cerebellum: implications for volume transmission. *J Neurophysiol* 70:2035–2044.
- Roitbak T, Syková E. 1999. Diffusion barriers evoked in the rat cortex by reactive astrogliosis. *Glia* 28:40–48.
- Rubin E, Farber JL. 1999. *Pathology*. 3rd ed. Philadelphia: Lippincott-Raven. 1513 p.
- Russell DS, Rubinstein LJ. 1977. *Pathology of tumors of the nervous system*. 4th ed. Baltimore: William & Wilkins. 317 p.
- Rutka JT, Myatt CA, Giblin JR, Davis RL, Rosenblum ML. 1987. Distribution of extracellular matrix proteins in primary human brain tumours: an immunohistochemical analysis. *Can J Neurol Sci* 14:25–30.
- Rutka JT, Apodaca G, Stern R, Rosenblum M. 1988. The extracellular matrix of the central and peripheral nervous systems: structure and function. *J Neurosurg* 69:155–170.
- Soroceanu L, Manning TJ Jr, Sontheimer H. 2001. Reduced expression of connexin-43 and functional gap junction coupling in human gliomas. *Glia* 33:107–117.
- Sugahara T, Korogi Y, Kochi M, Ikushima I, Shigematu Y, Hirai T, Okuda T, Liang L, Ge Y, Komohara Y, Ushio Y, Takahashi M. 1999. Usefulness of diffusion-weighted MRI with echo-planar technique in the evaluation of cellularity in gliomas. *J Magn Reson Imaging* 9:53–60.
- Syková E. 1992. Ion-selective electrodes. In: Stamford J, editor. *Monitoring neuronal cells: a practical approach*. New York: Oxford University Press. p 261–282.
- Syková E. 2001. Glial diffusion barriers during aging and pathological states. *Prog Brain Res* 132:339–363.
- Syková E, Svoboda J, Polák J, Chvátal A. 1994. Extracellular volume fraction and diffusion characteristics during progressive ischemia and terminal anoxia in the spinal cord of the rat. *J Cereb Blood Flow Metab* 14:301–311.
- Syková E, Mazel T, Šimonová Z. 1998. Diffusion constraints and neuron-glia interaction during aging. *Exp Gerontol* 33:837–851.
- Syková E, Vargová L, Prokopová Š, Šimonová Z. 1999. Glial swelling and astrogliosis produce diffusion barriers in the rat spinal cord. *Glia* 25:56–70.
- Syková E, Mazel T, Vargová L, Voříšek I, Prokopová-Kubinová. 2000. Extracellular space diffusion and pathological states. *Prog Brain Res* 125:155–178.
- Tien RD, Felsberg GJ, Friedman H, Brown M, MacFall J. 1994. MR imaging of high-grade cerebral gliomas: value of diffusion-weighted echoplanar pulse sequences. *AJR Am J Roentgenol* 162:671–677.
- Trosko JE, Ruch RJ. 1998. Cell-cell communication in carcinogenesis. *Front Biosci* 3:D208–236.
- Voříšek I, Hájek M, Tintěra J, Nicolay K, Syková E. 2002. Water ADC, extracellular space volume and tortuosity in the rat cortex after traumatic injury. *Magn Reson Med* 48:994–1003.
- Ye ZC, Rothstein JD, Sontheimer H. 1999. Compromised glutamate transport in human glioma cells: reduction-mislocalization of sodium-dependent glutamate transporters and enhanced activity of cystine-glutamate exchange. *J Neurosci* 19:10767–10777.
- Ye ZC, Sontheimer H. 1999. Glioma cells release excitotoxic concentrations of glutamate. *Cancer Res* 59:4383–4391.
- Zhang H, Kelly G, Zerillo C, Jaworski DM, Hockfield S. 1998. Expression of a cleaved brain-specific extracellular matrix protein mediates glioma cell invasion in vivo. *J Neurosci* 18:2370–2376.